to be submitted to J. Chem. Phys.

Analysis of the Near-Edge X-Ray-Absorption Fine-Structure of Anthracene: A Combined Theoretical and Experimental Study

Michael Klues[a], Klaus Hermann[b],* and Gregor Witte[a]†
[a] *Molekulare Festkörperphysik, Philipps-Universität Marburg, Germany*
[b] *Fritz-Haber-Institut der Max-Planck-Gesellschaft, Berlin, Germany*

The near-edge fine structure of the carbon K-edge absorption spectrum of anthracene was measured and theoretically analyzed by DFT calculations implemented in the StoBe code. It is demonstrated that the consideration of electronic relaxation of excited states around localized core holes yields a significant improvement of the calculated excitation energies and reproduces the experimentally observed fine structure well. The detailed analysis of excitation spectra calculated for each symmetry inequivalent excitation center allows in particular to examine the influence of chemical shifts and core hole effects on the excitation energies. Moreover, the visualization of final states explains the large variations in the oscillator strength of various transitions as well as the nature of Rydberg-states that exhibit a notable density of states below the ionization potentials.

Introduction

Near edge X-ray absorption spectroscopy (NEXAFS) is a sensitive method to study the electronic structure of unoccupied orbitals and bands in molecules and solids [1]. The probed transitions from core levels into empty or partially filled electronic states are element specific and very sensitive to the local bonding environment and coordination. Besides the characterization of molecular materials it has been extensively utilized to study properties of transition metal oxides, nitrides, carbides and sulfides [2]. NEXAFS has also become an important surface sensitive technique for studying the local electronic structure of adsorbed molecules [3–5]. Since corresponding transitions from core levels into unoccupied molecular orbitals are governed by dipole selection rules they also allow to determine the molecular orientation by analyzing the dichroism which occurs when the incidence angle and polarization direction of the linearly polarized synchrotron beam are varied. This structural analysis is particular advantageous as it does not require any crystalline ordering within the molecular films like in the case of X-ray diffraction analysis. Moreover, due to the high brightness of modern synchrotron sources such measurements can be readily carried out for adsorbates even at submonolayer coverage. The recent development in the field of organic electronics has led to a renewed interest in NEXAFS spectroscopy as an important tool to characterize the growth and structure of π-conjugated molecular materials [6–11]. Though the large lifetime of excitations into unoccupied π-orbitals in such materials give rise to rather sharp and distinct π*-resonances in the corresponding NEXAFS spectra, a precise assignment and identification of these signatures is required in order to fully exploit the potential of NEXAFS-based analyses. One approach to rationalize the resonances in NEXAFS spectra is based on tracing them back to characteristic signatures occurring in (small) aromatic molecules which are considered as building blocks of larger molecules and polymer materials. In fact, this building block principle has been successfully applied to polymers or oligomers where sub-molecular units are electronically decoupled, e.g. by single C-C bonds [12–15]. However, this approach is not applicable to larger fully conjugated aromatic molecules which, instead, exhibit a number of additional π*-resonances according to the size of the aromatic electron system [16–18]. This situation bears resemblance to the vibrational spectra of extended aromatic molecules, where collective, almost phononic vibrations appear instead of localized modes that are commonly used to identify functional units by fingerprints [19].

At present various theoretical approaches and computer codes to calculate NEXAFS spectra have become available which can also handle large aromatic hydrocarbons. These approaches differ essentially by the method to evaluate the electronic structure of the system under consideration. Here density-functional theory (DFT) codes, implemented e.g. in StoBe [20], deMon2k [21], or ADF [22], codes based on quantumchemical ab initio methods, implemented e.g. in CASSCF STOCKHOLM [23], or codes applying Green function methods, implemented e.g. in FEFF9 [24], are used.

It has been demonstrated that in many cases obtaining molecular NEXAFS signatures based on total densities of unoccupied states (DOUS) only is not fully conclusive [18]. The reason for this is the missing consideration of initial state effects which are due to differences in the C1s binding energies of differently coordinated carbon atoms within the molecule. Further, the impact of the various core hole locations on the wave function of the final states (i.e. electronic relaxation) and the influence of corresponding transition matrix elements can become important. Despite recent developments of modeling molecular NEXAFS spectra the number of detailed comparative studies is still very limited. Owing to technical chal-

lenges, experimental gas phase NEXAFS spectra which enable a direct comparison with calculations have been available only for very few aromatic molecules (including naphthalene and pentacene [25, 26]) and accurate calculations are restricted to single molecules because of their complexity. On the other hand, NEXAFS measurements of molecular multilayer films showed that the electronic structure of molecules in van der Waals bound solids remains largely unchanged [27] if compared with that of corresponding free molecules. This justifies comparisons of experimental NEXAFS spectra of the solids with those calculated for single free molecules. Note that, due to the intra-molecular nature of the X-ray absorption process in NEXAFS, the energy scale of measured spectra is not affected by surface potentials and work functions such as in the case of photoelectron spectroscopy. In contrast, significant geometric and electronic distortions occurring for chemisorbed molecules may yield significantly changed NEXAFS signatures for monolayer films in contact with metal substrates [3, 10, 28, 29].

Approximations used in the theoretical treatment of electron correlation and relaxation as well as the choice of basis sets can affect calculated NEXAFS spectra such that they have to be shifted by several eV to match corresponding experimental data [25, 26]. This can be overcome by appropriately choosing final state orbitals based on the transition potential approximation [30] together with a rather precise calculation of ionization energies to yield theoretical spectra which compare well with experimental data without requiring energetic corrections. These strategies, implemented in the DFT package StoBe [20], have been successfully applied for example to describe the electronic structure and NEXAFS spectra of different C_6-ring-containing molecules [31]. Here the similar coordination of the different carbon atoms as well as the limited size and high symmetry of such single ring hydrocarbons lead to rather small energy differences in the NEXAFS resonances. Therefore, larger aromatic systems with distinct shape anisotropy are required to compare and validate the theoretical approach.

In this work we have examined carbon K-edge NEXAFS spectra of anthracene ($C_{14}H_{10}$) which is a polycyclic aromatic hydrocarbon consisting of three fused benzene rings (cf. Fig. 4 a). Surprisingly, no high-resolution NEXAFS data (neither for gas-phase nor for solids) have been published so far for this acene. Only low-resolution NEXAFS spectra were reported for thin films adsorbed on Ag(111) and TiO_2(110) which in both cases reveal no distinct fine structure [32, 33]. To provide high resolution reference data without intensity variations of individual resonances due to orientational effects and to exclude electronic distortions owing to chemical interaction with the supporting substrate the present NEXAFS data were acquired for powder samples and are compared with calculated spectra. The spectra are further compared with previous NEXAFS experiments carried out for long-range ordered and highly oriented anthracene-based self-assembled monolayers (SAMs) [34] which reveal the influence of the anchoring unit on the NEXAFS signature of the aromatic backbone and also enable an experimental identification of π^*-resonances based on their dichroism. Interestingly, inner-shell electron energy loss spectroscopy (ISEELS) data have been obtained in a previous inelastic electron scattering experiment for gaseous anthracene which had also been simulated in the framework of detailed quantum chemical calculations [35]. Since for large electron impact energies such electronic excitation processes become similar to NEXAFS this enables an additional comparison. The aim of the present study is, on one hand, to validate the accuracy of the StoBe-based parameter-free calculations of NEXAFS spectra of larger aromatic molecules and, on the other hand, to illustrate relaxation effects and explain pronounced variations of the oscillator strength for the individual NEXAFS resonances which is particular important for extended π-conjugated systems.

Methodology

Experimental Details. Since the low sublimation enthalpy and resulting high vapor pressure of anthracene hampers the preparation of thin films by evaporation from Knudsen cells samples were prepared by reaming thin films of high purity anthracene (ACROS organics, purity 99 %) onto a scarified copper plate which was rapidly cooled below 150 K after loading the sample holder into the UHV-chamber. The carbon K-edge NEXAFS measurements were carried out at the HE-SGM dipole beamline of the synchrotron storage ring facility BESSY II in Berlin (Germany). A retarding field analyzer with a suppressor field of 60 eV was used for partial electron yield (PEY) detection of secondary electrons as a function of the photon energy of the linearly polarized incident synchrotron light (polarization factor 91%). The exit slit of the grating monochromator was chosen such that a spectral width of the incident light was 300 meV achieved. The absolute energy scale of the NEXAFS spectra was calibrated by simultaneously recording the photocurrent from a carbon coated gold grid in the incident beam which exhibits a sharp resonance at 284.9 eV as cross-calibrated by means of a graphite sample. The raw NEXAFS data have been normalized with respect to the incident photon flux and considering the energy dependent transmission characteristic of the monochromator grating.

Computational Approach. The work flow describing all individual steps of the present DFT calculations of carbon edge NEXAFS spectra based on the StoBe package [20] is depicted in Fig.1. In the first step the molecular structure of the free anthracene molecule is optimized using the gradient-corrected revised Perdew-

Burke-Ernzerhof (RPBE) functional [36, 37] and all-electron triple-zeta valence plus polarization basis sets (TZVP) [38]. The same functional and basis sets are also used in all further steps. This first step yields, apart from the equilibrium geometry, also information about the electronic ground state of the molecule. While in the geometry optimizations all carbon atoms are described by identical all-electron basis sets the following calculations of ionized and core excited states use basis sets which differ between the respective excitation carbon and the other spectator carbon centers. For the excitation carbon a basis set of IGLO-III quality [39] is applied to adequately describe inner shell relaxation effects while the other carbon centers are accounted for by effective core potentials (ECPs) for the 1s shell and [3s3p1d] valence basis sets to avoid 1s core orbital mixing [40, 41].

Anthracene includes four types of carbon atoms (C_i) which are non-equivalent by symmetry and exposed to a slightly different chemical environment as indicated in Fig. 4 a. Thus, the above choice of basis sets is used in four different calculations of ground and C 1s hole states which yield corresponding total energies $E_{GS}(C_i)$ and $E_{IS}(C_i)$ where the difference $IP_i = E_{IS}(C_i)$ - $E_{GS}(C_i)$ defines the fully relaxed ionization potential (ΔSCF value) of the corresponding carbon atom C_i, $i = 1...4$. The resulting IP values are corrected further by a shift of 0.4 eV to higher energies to account for relativistic effects [42].

In the next step we consider carbon 1s core excitations into unoccupied final state orbitals where the latter are determined, for each of the four different carbon species, in one self-consistent calculation based on the transition potential approximation [30]. In this approach the electronic structure of the molecule is evaluated self-consistently where the corresponding C 1s orbital is occupied by only half an electron to account for electronic relaxation during the excitation process. The resulting unoccupied orbitals are then used as approximate final state orbitals in the evaluation of dipole transitions from the C 1s core orbital with transition moments determining the spectral oscillator strengths and Kohn-Sham eigenvalue differences yielding approximate excitation energies to describe the theoretical NEXAFS spectrum in a first approximation. In order to account for transitions into diffuse Rydberg states and final states beyond ionization the basis set at the carbon excitation center is augmented by a large set, [19s19p19d], of diffuse basis functions following a double basis set technique [17, 43]. The NEXAFS spectrum for each non-equivalent carbon atom obtained so far needs to be improved further. First, the C 1s ionization potential obtained within the transition potential framework, which is identical with that obtained by Slater's transition state method [44], includes only limited electronic relaxation. Thus, its value is larger by about 1 eV compared with the fully relaxed ΔSCF result. This can be corrected by

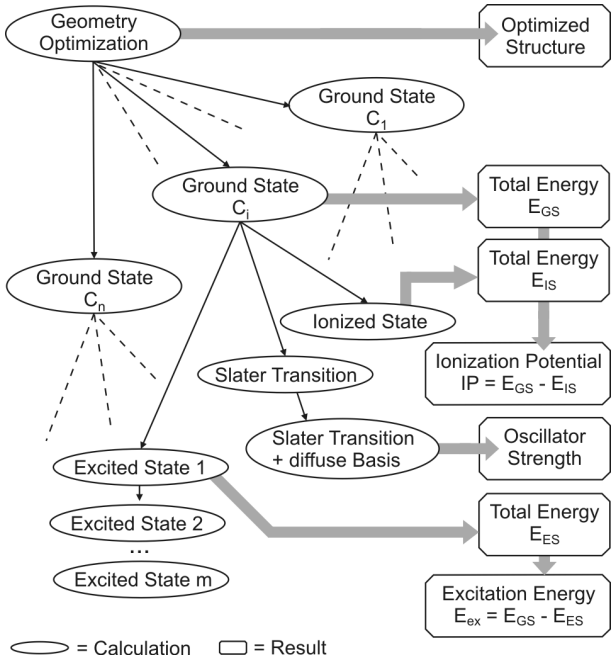

FIG. 1: Schematic flowchart of DFT-based calculations of carbon K-edge NEXAFS spectra carried out within the StoBe-package (for details see text). The angular boxes on the right hand side represent the results of the individual steps of the iterations. C_i denotes the position of core hole excitation among the symmetry non-equivalent carbon positions, while m indicates the number of excited state which has to be considered for every center C_i.

applying a rigid shift to the NEXAFS spectrum obtained by the transition potential approximation which compensates the difference. Second, more reliable excitation energies can be obtained by explicit self-consistent calculations of excited states with the electron of a C 1s core orbital transferred to an unoccupied orbital of the ground state. Then the difference of the total energy of the excited state and that of the ground state determines the fully relaxed excitation energy, analogous to the ΔSCF procedure described above. For the present anthracene molecule this evaluation has been performed for the lowest fifteen excitations starting from the 1s core orbital of each of the four non-equivalent carbon atoms. For better convergence of the self-consistent calculations, virtual orbitals below the highest occupied orbital of higher excited states are restricted from orbital rotations by applying appropriate supersymmetry constraints. The improved excitation energy spectrum is then complemented with the corresponding dipole transition moment from the transition potential calculations to arrive at a final theoretical NEXAFS spectrum.

To account for the finite experimental resolution and to enable a comparison with measured NEXAFS spectra the calculated transition energies are convoluted by Gaussians of full-width-at-half-maximum (FWHM) amount-

ing to 0.5 eV for π^*-type and 0.7 eV for σ^*- or Rydberg-type resonances based on empirical values from experiment. Visualization of orbitals was performed with MacMolPlt [45].

Results

Experimental C1s NEXAFS-spectra of Anthracene. The experimental carbon K-edge NEXAFS data of anthracene are summarized in Fig. 2. Characteristic signatures are two intense and sharp peaks at 284.5 eV and 285.8 eV accompanied by low intensity shoulders at higher energy, somewhat broader and partially overlapping peaks between 287.5 and 290 eV as well as substantially broader peaks around 294 and 300 eV. Based on their width and energetic positions relative to the ionization threshold (which typically amounts to about 290 eV for conjugated hydrocarbons [26]) the sharp peaks can be assigned to excitations into unoccupied π^* orbitals while the latter broad peaks are attributed to excitations into σ^* orbitals [46]. To facilitate comparison with calculated absorption spectra the additional electron signal due to Auger deexcitation of core holes created by photoemission (so called *absorption edge*) has been subtracted. As described in [1] this edge can be modeled by assuming that the electron emission rate is determined essentially by the lifetime of the core hole. Considering a Lorentzian line shape for the core level excitation this yields an analytical expression for the step edge in form of an *arc tangent* function [47]. More precisely, the edge is actually a superposition of several overlapping step functions, since every non-equivalent carbon atom within the molecule has a slightly different ionization potential which makes the exact position of the absorption edge and its shape hard to quantify in experiment. Therefore, the adsorption edge shown in the inset of Fig. 2 was constructed from the ionization potentials calculated for the symmetry non-equivalent carbon atoms (see below) taking into account their multiplicity and using an empirical peak width of 0.5 eV.

Due to the isotropic molecular orientation in powders the intensity of individual NEXAFS resonances are independent on the orientation of the electrical field vector **E** of the incident synchrotron light, hence, offering an ideal reference system to examine the free molecule NEXAFS signature. In contrast, NEXAFS spectra of oriented films of π-conjugated molecules exhibit a noticeable dichroism of π^* resonances which enables a quantitative characterization of molecular orientation [6–11]. This approach exploits the fact that the intensity of π^* resonances depend on the relative orientation of **E** according to $I(\pi*) \propto |\mathbf{E} \cdot \mathbf{T}|^2$, where **T** denotes the transition dipole moment which is oriented normal to the ring plane of aromatic molecules [1]. In a previous study it has been shown that aromatic self-assembled monolayers

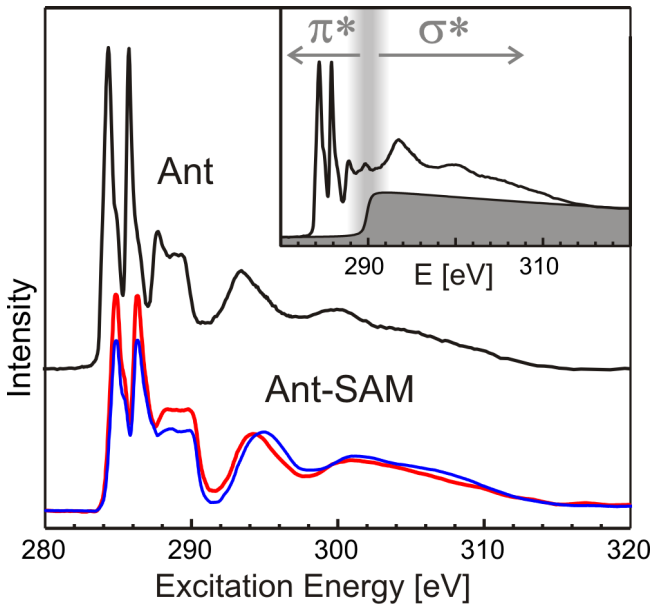

FIG. 2: C K-edge NEXAFS spectra of anthracene powder (black curve) and an anthraceneselenolate-SAM on Au(111) after subtracting a K-edge. The used K-edge as well as a raw spectrum before edge subtraction are shown in the inset. A notable dichroism occurs for the SAM yielding intensity variations of the π^* resonances for different photon polarization (red curve: perpendicular incidence, blue curve: grazing incidence).

(SAMs) with anthracene backbones can be prepared with remarkable long-range ordering when selenolates are used as anchoring groups [34]. Therefore, the corresponding NEXAFS data of an anthraceneselenolate SAM are included for comparison in Fig. 2. Interestingly, the SAM reveals virtually the same NEXAFS signature as the anthracene powder which reflects the electronic decoupling of the aromatic backbone and the anchoring unit. However, a noticeable dichroism is found for resonances with energies below 290 eV (red curve: perpendicular beam incidence, blue curve: grazing incidence, θ=30°) which reflects a distinct directional ordering. The quantitative analysis of the dichroism obtained in spectra taken at different angles of incidence of the synchrotron light yields an average angle of **T** relative to the surface normal of θ=59° (for details of the analysis see [34]). In order to determine the orientation of the anthracene backbone also the herringbone packing motif within the film has to be taken into account. Employing the analysis shown in [49] this yields, altogether, an angle of 33° between the anthracene backbone plane and the surface normal.

Calculated NEXAFS-spectra. As depicted in Fig. 3) the total NEXAFS spectrum of anthracene calculated by the transition potential method is already in close agreement with the experimental data. Characteristic features such as the intense resonance doublet in the pre-edge region as well as broad resonances at energies

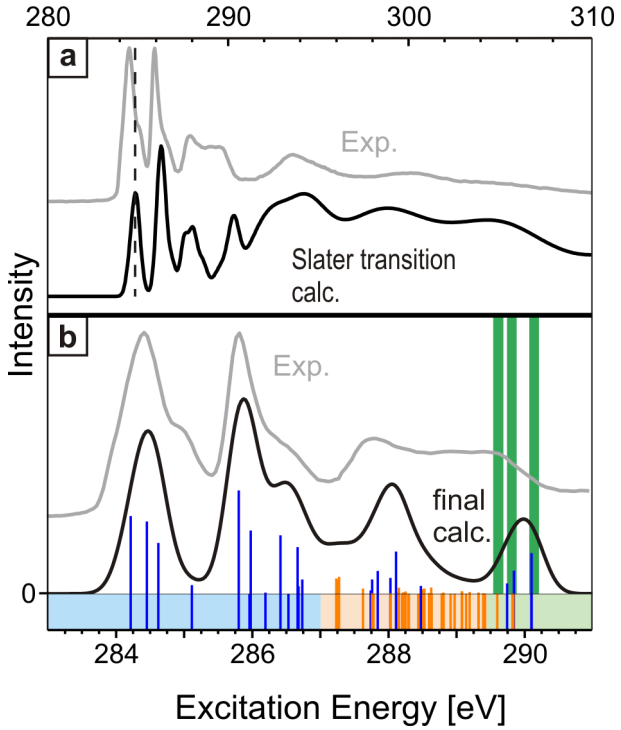

FIG. 3: Comparison of experimental and theoretical data with different levels of approximation. (a) Full spectrum resulting from transition potential calculations compared with experimental data. (b) NEXAFS spectrum of the pre-edge region including full electronic relaxation from a weighted superposition of the partial spectra (cf. Fig. 4) according to the multiplicity of the excitation centers compared with experimental data

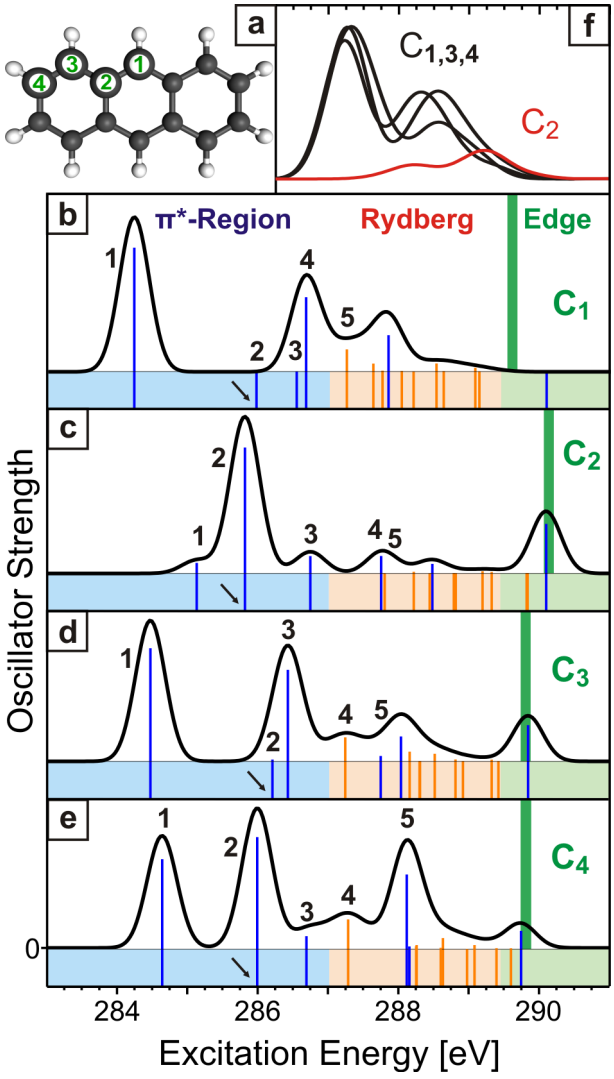

FIG. 4: Summary of calculated C 1s NEXAFS spectra of anthracene. (a) Structure of Anthracene. Numbered carbon atoms were used as excitation centers for calculations (b-e) Partial NEXAFS spectra calculated for each symmetry non-equivalent carbon center (C_1 - C_4) including full electronic relaxation (see text). The color code denotes the character of the corresponding final states (blue: π^* orbitals, orange: Rydberg states) while the green bars indicate the ionization potentials of the symmetry non-equivalent carbon centers sketched in a. Small arrows point at excitations which are treated in Fig. 5. Note that the oscillator strengths of the various partial spectra are not to scale; (f) Compilation of the partial NEXAFS spectra of b-e for excitations in the Rydberg region (see text).

higher than the absorption edge, corresponding to excitations into antibonding σ^*(C-C) orbitals, are reproduced reasonably. However, a closer look reveals also differences. The calculated energies of the leading peaks are too high and their intensity ratio is not correctly reproduced. Moreover, the experimental data exhibit shoulders in the high energy flank of these peaks which are missing in the calculations as well as the intensity around 289 eV. Since the excited molecular states at high energies are inherently difficult to calculate, and according to their very short lifetime yield only extremely broad signals, we will focus on the low-energy part of the NEXAFS spectrum below the ionization potential. Further more this energy region is of special interest because the corresponding states are sensitive to chemical changes and can be used for dichroitic measurements.

As discussed above, the theoretical NEXAFS spectra can be improved beyond the transition potential approximation by explicitly evaluating core excited final states of the molecule. As a result, Figs. 4 b-e shows partial NEXAFS spectra for the four different carbon atoms C_1 to C_4 in anthracene where the lowest fifteen excited states have been considered. In these spectra the vertical lines indicate the excitation energies determined from total energies of the fully relaxed excited final and corresponding ground states. Lines which extend above the color bar reflect excitations with relatively large transition moments with their lengths characterizing the moment size while those completely inside the color bar describe transitions of negligible moments. In addition, the painting of the

color bar denotes the different character of the final state orbitals where blue and orange refer to π*-orbitals and Rydberg-orbitals, respectively. The thick vertical green lines indicates the ionization thresholds of the different carbon atoms in the molecule exhibiting only small variations (*chemical shifts*) of less than or equal to 0.5 eV, see also Tab.I. Finally, the continuous curves in Figs. 4 b-e describe the corresponding discrete energy spectra convoluted by gaussian broadening to give an experimental appearence, see above.

TABLE I: Calculated ionization potentials (IP in eV) of the four symmetry non-equivalent carbon atoms in anthracene (cf. Fig. 4 a)

	C_1	C_2	C_3	C_4
IP [eV]	289.6	290.1	289.8	289.8

Common to all partial NEXAFS spectra, calculated for the different symmetry non-equivalent carbon atoms, are several less intense peaks at energies 0-3 eV below ionization threshold which are assigned to excitations into Rydberg-type final state orbitals (orange bars) which are spatially extended and of anti-bonding σ(C-H) character. These excitations are energetically well separated from more intense excitations (blue bars) at lower energy. The energetically lowest unoccupied orbitals above the LUMO of aromatic molecules are found to be almost always π-type which is also true for anthracene. Thus, the blue energy region of the spectrum is characterized by excitations into π-type orbitals (π*-region). The partial NEXAFS spectra of the different carbon atoms can be superimposed according to their multiplicity to yield a total NEXAFS spectrum of the molecule to be compared with the measured spectrum after edge subtraction as shown in Fig. 3 b).

TABLE II: Lowest five excitation energies calculated for the four symmetry non-equivalent carbon atoms in anthracene. All energies are given in eV.

Excitation	C_1	C_2	C_3	C_4
1	284.2	285.1	284.5	284.6
2	286.0	285.8	286.2	286.0
3	286.5	286.7	286.4	286.7
4	286.7	287.8	287.2	287.3
5	287.3	287.8	287.7	288.1

Discussion

Obviously, the calculated total NEXAFS spectrum, see Fig. 3 b, agrees quite closely with the experimental data. All fine structures are well reproduced and the energetic position of the resonances agree within 0.3 eV. Moreover,

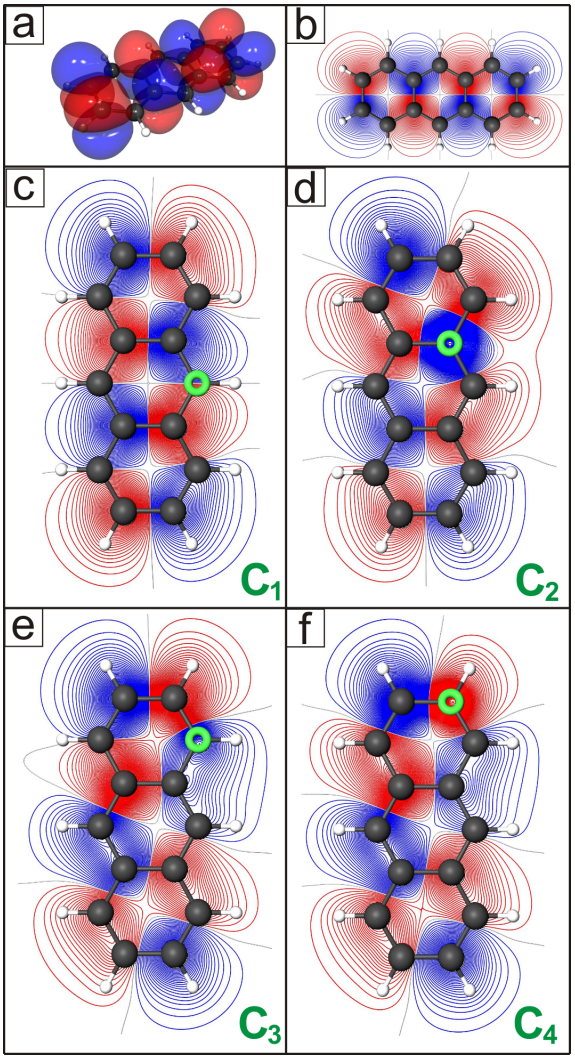

FIG. 5: Visualization of the LUMO+1 orbital in anthracene. (a) Iso-surface and (b) contour plot calculated for the ground state. The contour plane refers to a cut 0.5 Å below the plane through the atom centers. Positive and negative orbital values are shown in blue and red, respectively; (c), (d), (e), (f) Contour plot as in (b) but calculated for the excited final state with holes at C_1, C_2, C_3 or C_4. The contour lines in (c) - (f) refer to identical values and corresponding excitation centers are labeled by green toruses.

the theoretical analysis provides detailed insight into the character of the different excitations which can explain the size of their oscillator strengths.

The calculated partial excitation spectra shown in Figs. 4 b-e reveal, depending on the transitions, very different oscillator strengths which can be understood by the symmetry of the corresponding final state orbitals. This is illustrated in Fig. 5 for carbon core excitations into the second lowest unoccupied (LUMO+1) final state orbital (indicated by arrows in Figs. 4 b-e) starting from the different carbon atoms. The LUMO+1 orbital of the anthracene ground state, see Fig. 5 a and b, is of π*-type

and described by an anti-bonding arrangement of C 2p orbitals perpendicular to the molecular plane and located at the inner eight carbon centers. This includes centers C_2, C_4 but excludes C_1, C_3. The orbitals of the core excited states corresponding to LUMO+1, see Figs. 5 c-f, are somewhat distorted due to the core hole but still resemble that of the ground state. Thus, dipole transition matrix elements of the C 1s with corresponding final state LUMO+1 orbitals involve integration over products of the dipole operator with C 1s and 2p contributions at the respective carbon center which yield finite values for matrix elements at the inner eight carbon centers, such as C_2, C_4. In contrast, matrix elements at the outer six carbon centers, such as C_1, C_3, assume very small values. As a consequence, the oscillator strengths of the corresponding transitions are large for excitations at C_2, C_4 but small at C_1, C_3 as evidenced in Figs. 4 b-e.

The dependence of the partial NEXAFS spectra on the shape of final state orbitals is also evident for core excitations involving rather extended Rydberg-type final state orbitals as shown in Fig. 4 f). While the partial spectra belonging to transitions from excitation centers C_1, C_3 and C_4 (black) yield nearly the same energy dependence of the spectral intensity the excitation spectrum for center C_2 (red) is rather different which is explained by the binding environment of the C_2 atom. Compared with the other carbon atoms, C_2 does not include a neighboring hydrogen to form a local C-H bond. However, Rydberg-type orbitals in athracene are characterized by sizeable σ^*(C-H) contributions from carbon centers other than C_2. This is illustrated in Fig. 6 which compares the LUMO+4 Rydberg orbital of the ground state, Fig. 6 a, with corresponding orbitals of the core excited states, Figs. 6 b,c, containing holes at the carbon centers C_1 and C_2, respectively. Obviously, the final state orbital of the C_1 core excitation, Fig. 6 b, shows a density near the C_1 center (due anti-bonding C-H contributions) which is larger than for the respective orbital of the C_2 core excitation near the C_2 center. As a consequence, the dipole transition moment of the excitation no. 5 is larger in the C_1 than the C_2 derived partial NEXAFS spectrum which is confirmed in Figs. 4 b,c.

The carbon K-edge NEXAFS spectrum of anthracene has been calculated earlier by Ågren et al. [16] using the static exchange approach. While the general characteristics observed in the experimental data were roughly reproduced relative peak intensities were not well described. In particular, the calculated positions of the leading π^* resonances differ from the experiment by about 1.5 eV. The comparison of the experimental with the present theoretical spectra at different levels of approximation, transition potential vs. fully relaxed final state spectra, see Figs. 3 and b, may explain these discrepancies. Our results suggest that electronic relaxation in the final states due to the changed coulomb potential caused by the core hole is a key element to obtain

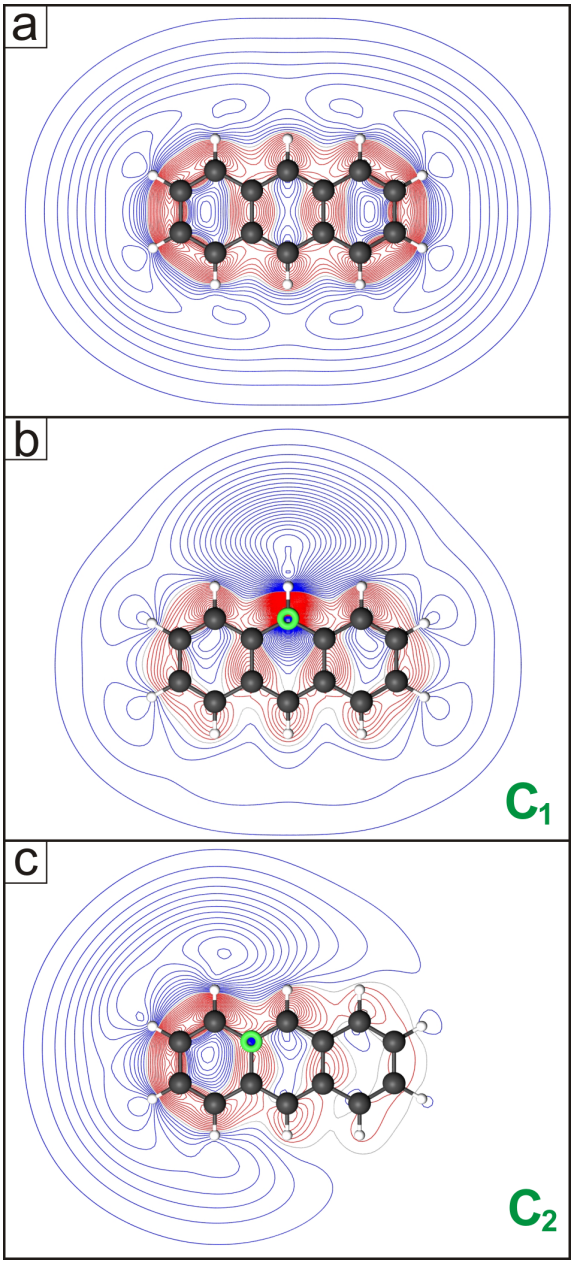

FIG. 6: Visualization of the LUMO+4 orbital in anthracene. (a) Contour plot calculated for the ground state along the molecular plane. Positive and negative orbital values are shown in blue and red, respectively; (b), (c) Contour plot as in (a) but calculated for the excited final state with a C_1 and C_2 hole. The contour lines in (a) - (c) refer to identical values, also used in Fig. 5, and corresponding excitation centers are labelled by green toruses. The final state orbitals of (b), (c) correspond to excitations no. 5 in Fig. 4 b,c).

precise excitation spectra. As shown in Fig. 5 core hole screening can lead to noticeable distortion of the final state orbitals shifting nodal planes which affect the transition matrix elements. Further, low-lying excitation energies in the fully relaxed spectrum, Fig. 3 b, are shifted by about 1 eV when compared to the transition potential

spectrum, Fig. 3 a, where the shift values vary by up to 0.5 eV for different excitations.

Core hole screening can also affect the energetic order of excitations in the spectrum depending on the excitation center. This is illustrated by a comparison of the fully relaxed partial NEXAFS spectrum for the C_1 center, Fig. 4 b, with that for the C_3 center, Fig. 4 d. While the C_1 derived spectrum includes four π^*-type excitations in the low-energy region before excitations to Rydberg final states appear, the C_3 derived spectrum offers only three with the energy regions of π^*- and Rydberg-type excitations overlapping. This substantiates the importance of core hole screening which influences the NEXAFS spectra differently depending on the location and chemical environment of the excitation center. It is consistent with earlier work by by Oji et al. [18] and may callenge the validity of a constant energetic shift used in the static exchange approach [16, 26].

The analysis of the partial NEXAFS spectra calculated for different carbon excitation centers allows also to estimate the influence of site specific initial state effects due to chemical binding. A comparison of the IP values of the four different carbon atoms in athracene, cp. Tab. I, reveals minor variations with the largest value refering to atom C_2. The latter seems plausible since C_2 has three carbon and no hydrogen neighbor while C_1, C_3, and C_4 all have two carbon and one hydrogen neighbor. Considering that the electronegativity of carbon is slightly higher than for hydrogen, this yields a somewhat reduced electron density at C_2 if compared with the other C_i species. Thus, there is a smaller shielding of the core charge in the initial state for C_2 which suggests a larger ionization energy. On the other hand, the IP value of C_2 is larger than that for C_1 by 0.5 eV, see Tab. I, while the first core hole excitation energies of the two atoms differ by 0.9 eV, see Tab. II. This indicates that only part of the difference in the excitation energies can be attributed to inital state effects. Together with the appearance of several pronounced π^* resonances within the same partial NEXAFS spectrum (involving the same carbon core hole), it demonstrates that the leading π^* doublet structure of anthracene cannot be attributed exclusively to core excitations at different carbon atoms into a LUMO-based final state as suggested earlier [16].

Since the lowest unoccupied molecular orbitals of aromatic molecules are usually of π character the leading NEXAFS resonances are often attributed to excitations into π-type LUMO, LUMO+1, etc. orbitals where orbitals of the molecular ground state are considered. This simplified picture ignores, however, substantial variations in the dipole transition moments which sometimes lead to vanishing oscillator strength as discussed for the second π^* resonance in the partial NEXAFS spectra (cf. Fig. 4b-e). This demonstrates that an assignment of molecular orbitals to final states of excitation solely based on the order of the respective subresonance is not possible and instead requires a detailed theoretical analysis.

Though we find quite good overall agreement of the calculated total NEXAFS spectrum of anthracene with measured data, as shown in Fig. 3, there are still some small deviations. The most prominent difference between theory and experiment is the missing shoulder in the high energy flank of the lowest excitation peak. In previous experiments additonal fine structures have been observed in high resolution NEXAFS spectra which were identified as coupling of the electronic transitions to various vibronic excitations [50, 51]. These features have only been observed in gas phase C K-edge NEXAFS spectra of small aromatic hydrocarbons or in O K-edge NEXAFS spectra of substituted aromatic molecules, which suggests an efficient coupling to C=O stretching mode, while they have not been observed in any C K-edge NEXAFS data of condensed aromatic molecules. Therefore it appears unlikely that the extra shoulder occurring in the high energy flank of the lowest excitation peak results from a vibrational excitation. Further, there is missing intensity in the energy region between 288 eV and 290 eV characterizing Rydberg excitations. The origin of these differences can be manifold. First, in the present theoretical study we evaluate fully relaxed excitation energies whereas for the dipole transition moments, determining spectral intensities, we restrict ourselves to values obtained in the transition potential approximation which accounts only for limited electronic relaxation. This can be improved by calculating electron transition moments with fully relaxed final state wavefunctions. Second, basis set influences in the description of the molecular Rydberg-type orbitals and their consequences for corresponding excitations may have to be examined in detail. Third, multi-electron excitations ignored by the present theoretical description cannot be fully excluded in the experiment. Studies along these lines are currently under way.

Conclusions

The present combined theoretical and experimental study shows that carbon K-edge NEXAFS spectra of π-conjugated molecules can be calculated rather precisely when taking into account relaxation effects of final states caused by excitations from localized hole states. The aproach implemented in the StoBe package has been validated for the anthracene molecule where an agreement between the measured and calculated peak positions of about 0.3 eV is found. The high accuracy in the calculation of ionization potentials of the different carbon atoms within the molecule allows, in particular, a reliable modelling of the absorption edge which can be subtracted from the measured spectra in order to identify further resonances that are overlapping with the edge jump. Such refined analyses are particularly useful for aromatic molecules containing heteroatoms where initial

and final state effects become even more important. In that case several energetically well separated edges occur leading to sizeable overlap of some NEXAFS resonances with the edges. The ability to appropriately analyse NEXAFS signatures will also be of importance for future experiments on multinary molecular systems where an accurate understanding of the individual components is required to examine possible intermolecular coupling.

Acknowledgement We acknowledge the Helmholtz-Zentrum Berlin - Electron storage ring BESSY II for providing synchrotron radiation at beam line HE-SGM and for travel support.

* Electronic address: hermann@FHI-Berlin.MPG.de
† Electronic address: gregor.witte@physik.uni-marburg.de

[1] Stöhr, J. In *NEXAFS Spectroscopy*; Gomer, R., Ed.; Springer, 1992.
[2] Chen, J. G. *Surf. Sci. Rep.* **1997**, *30*, 1-152.
[3] Weiss, K.; Gebert, S.; Wühn, M.; Wadepohl, H.; Wöll, C. *J. Vac. Sci. Technol.,A* **1998**, *16*, 1017-1022.
[4] Triguero, L.; Luo, Y.; Pettersson, L. G. M.; Ågren, H.; Väterlein, P.; Weinelt, M.; Fröhlisch, A.; Hasselström, J.; Karis, O.; Nilsson, A. *Phys. Rev. B* **1999**, *59*, 5189-5200.
[5] Hähner, G. *Chem. Soc. Rev.* **2006**, *35*, 1244-1255.
[6] Umbach, E.; Glockler, K.; Sokolowski, M. *Surf. Sci.* **1998**, *402*, 20-31.
[7] Frey, S.; Stadler, V.; Heister, K.; Eck, W.; Zharnikov, M.; Grunze, M.; Zeysing, B.; Terfort, A. *Langmuir.* **2001**, *17*, 2408-2415.
[8] Kera, S.; Casu, M.B.; Bauchspiess, K.R.; Batchelor, D.; Schmidt, T.; Umbach, E. *Surf. Sci.* **2006**, *600*, 1077-1084.
[9] Peisert, H.; Biswas, I.; Zhang, L.; Knupfer, M.; Hanack, M.; Dini, D.; Batchelor, D.; Chasse, T. *Surf. Sci.* **2006**, *600*, 4024-4029.
[10] Käfer, D.; Witte, G. *Chem. Phys. Lett.* **2007**, *442*, 376-383.
[11] Chen, W.; Qi, D.C.; Huang, Y.L.; Huang, H.; Wang, Y.Z.; Chen, S.; Gao, X.Y.; Wee, A.T.S. *J. Phys. Chem. C* **2009**, *113*, 12832-12839.
[12] Urquhart, S. G.; Hitchcock, A. P.; Smith, A. P.; Ade, H. W.; Lidy, W.; Rightor, E. G.; Mitchell, G. E. *J. Electron. Spectrosc. Relat. Phenom.* **1999**, *100*, 119-135.
[13] Pettersson, L. G. M.; Ågren, H.; Schürmann, B. L.; Lippitz, A.; Unger, W. E. S.; *Int. J. Quantum Chem. B* **1996**, *63*, 749-765.
[14] Unger, W. E. S.; Lippitz, A.; Wöll, C.; Heckmann, W. *Fresenius J. Anal. Chem.* **1997**, *358*, 89-92.
[15] Käfer, D.; Ruppel, L.; Witte, G.; Wöll, C. *Phys. Rev. Lett.* **2005**, *95*, 166602.
[16] Ågren, H.; Vahtras, O.; Carravetta, V. *Chem. Phys.* **1995**, *196*, 47-58.
[17] Ågren, H.; Carravetta, V.; Vahtras, O.; L.G.M. Pettersson *Theor. Chem. Acc.* **1997**, *97*, 14-40.
[18] Oji, H.; Mitsumoto, R.; Ito, E.; Ishii, H.; Ouchi, Y. *J. Chem. Phys.* **1998**, *109*, 10409.
[19] Breuer, T.; Celik, M. A.; Jakob, P.; Tonner, R.; Witte, G.; *J. Phys. Chem. C.* **2012**, *116*, 22652.
[20] Hermann, K.; Pettersson, L. G. M.; Casida, M. E.; Daul, C.; Goursot, A.; Koester, A.; Proynov, E.; St-Amant, A.; Salahub. D. R.; Contributing authors: Carravetta, V.; Duarte, H.; Friedrich, C.; Godbout, N.; Guan, J.; Jamorski, C. ; Leboeuf, M.; Leetmaa, M.; Nyberg, M.; Patchkovskii, S.; Pedocchi, L.; Sim, F.; Triguero, L.; Vela. A. *StoBe-deMon version 3.2,* **2013**.
[21] Köster, A. M.; Geudtner, G.; Calaminici, P.; Casida, M. E.; Dominguez, R.; Flores-Moreno, R.; Gamboa, G. U.; Goursot, A.; Heine, T.; Ipatov, A.; Janetzko, F.; del Campo, J. M.; Reveles, J. U.; Vela. A.; Zuniga-Gutierrez, B.; Salahub. D. R.; *deMon2k version 4,* **2013**.
[22] ADF2013, SCM, Theoretical Chemistry, Vrije Universiteit, Amsterdam, The Netherlands, *http://www.scm.com.*
[23] Pettersson, L. G. M.; Ågren, H.; Vahtras, O.; Carravetta, V. *J. Chem. Phys.* **1995**, *103*, 8713.
[24] Rehr, J. J.; Kas, J. J.; Vila, F. D.; Prange, M. P.; Jorissen, K. *Phys. Chem. Chem. Phys.* **2010**, *12*, 5503-5513.
[25] Hollauer, E.; dos Santos Prucole, E.; Rocco, M. L. M.; Netto, A. D. P.; Schöll, A.; Fink, R.; *J. Braz. Chem. Soc.* **2005**, *16*, 31-36.
[26] Alagia, M.; Baldacchini, C.; Betti, M. G.; Bussolotti, F.; Caravetta, V.; Ekström, U.; Mariani, C.; Stranges, S. *J. Chem. Phys.* **2005**, *122*, 124305.
[27] Käfer, D.; Ruppel, L.; Witte, G. *Phys. Rev. B* **2007**, *75*, 085309.
[28] Hasselström, J.; Karis, O.; Weinelt, M.; Wassdahl, N.; Nilsson, A.; Nyberg, M.; Pettersson, L. G. M.; Samant, M. G.; Stöhr, J. *Surf. Sci.* **1998**, *407*, 221-236.
[29] Qui, D. C.; Chen, W.; Wee, A. T. S. in *The Molecule-Metal Interface* (Eds. N. Koch, N. Ueno and A. T. S. Wee); Wiley-VCH, 2013.
[30] Triguero, L.; Pettersson, L. G. M.; Ågren, H. *Phys. Rev. B* **1998**, *58*, 8097-8110.
[31] Kolczewski, C.; Püttner, R.; Martins, M.; Schlachter, A. S.; Snell, G. *J. Chem. Phys.* **2006**, *124*, 034302.
[32] Reiß, S.; Krumm, H.; Niklewski, A.; Staemmler, V.; Wöll, C. *J. Chem. Phys.* **2002**, *116*, 7704.
[33] Yannoulis, P.; Frank, K. H.; Koch, E. E.; *Surf. Sci.* **1991**, *241*, 325-334.
[34] Bashir, A.; Käfer, D.; Müller, J.; Wöll, C.; Terfort, A.; Witte, G, *Angew. Chem.* **2008**, *47*, 5250.
[35] Gordon, M. L.; Tulumello, D.; Cooper, G.; Hitchcock, A. P.; Glatzel, P.; Mullins, O. C.; Cramer, S. P.; Bergmann, U. *J. Phys. Chem. A* **2003**, *107*, 8512-8520.
[36] Hammer, B.; Hansen, L. B.; Norskov, J. K. *Phys. Rev. B* **1999**, *59*, 7413-7421.
[37] Perdew, J. P.; Burke, K.; Ernzerhof, M. *Phys. Rev. Lett.* **1996**, *77*, 3865-3868.
[38] Godbout, N.; Salahub, D. R.; Andzelm, J.; Wimmer, E. *Can. J. Chem* **1992**, *70*, 560.
[39] Kutzelnigg, W.; Fleischer, U.; Schindler, M. *NMR-Basic Principles and Progress (Springer, Heidelberg)* **1990**, *23*, 165.
[40] Nyberg, M. Ph.D. Thesis, Stockholm University, 2000.
[41] Pettersson, L. G. M.; Wahlgren, U.; Gropen, O. J. *J. Chem. Phys.* **1987**, *86*, 2176-2184.
[42] Triguero, L.; Plashkevych, O.; Pettersson, L., G., M.; Ågren, H. *J. Electron. Spectrosc. Relat. Phenom.* **1999**, *104*, 195.
[43] Ågren, H.; Carravetta, V.; Vahtras, O.; Petters-

son, L. G. M. *Chem. Phys. Lett.* **1994**, *222*, 75-81.
[44] Slater, J., C.; Johnson, K., H. *Phys. Rev. B* **1972**, *5*, 844.
[45] Bode, B. M.; Gordon, M. S. in *J. Mol. Graphics Modell.* **1998**, *16*, 133-138
[46] Yokoyama, T.; Seki, K.; Morisada, I.; Edamatsu, K.; Ohta, T., *Phys. Scr.* **1990**, *41*, 169.
[47] As shown in [1] the measured absorption edge can be modeled by the expression: $I_{edge} = H[\frac{1}{2} + \frac{1}{\pi}arctan(\frac{E-IP}{\Gamma/2})] \times exp(-d(E - IP - \Gamma))$, where H, E, IP and Γ denote the edge jump intensity, photon energy, ionization potential and spectral resolution, respectively. The second factor accounts for the energy dependent photoionization cross section for photon energies larger than the ionization potential [48].
[48] Henke, B.L.; Gullikson, E.M.; Davis, J.C. , *At. Data Nucl. Data Tables* **1993**, *54*, 181.
[49] Käfer, D.; Witte, G.; Cyganik, P.; Terfort, A.; Wöll, Ch. *J. Am. Chem. Soc.* **2006**, *128*, 1723.
[50] Hübner D.; Holch, F. ; Rocco, M.L.M.; Prince, K.C.; Stranges, S.; Schöll, A.; Umbach, E.; Fink, R., *Chem. Phys. Lett.* **2005**, *415*, 188.
[51] Schmidt, N.; Clark, T.; Urquhart, S.G.; Fink, R.H., *J. Chem. Phys.* **2011**, *135*,144301.